Extinction-ice water content-effective radius algorithms for CALIPSO

Andrew J. Heymsfield
National Center for Atmospheric Research, Boulder, Colorado, USA

Dave Winker
NASA Langley Research Center, Hampton, Virginia, USA

Gerd-Jan van Zadelhoff
Koninklijk Nederlands Meteorologisch Instituut, De Bilt, Netherlands

Received 17 February 2005; revised 7 April 2005; accepted 20 April 2005; published 20 May 2005.

[1] Interrelationships between volume extinction coefficient (σ), ice water content (IWC), and effective radius (r_e), each dependent upon the particle size distribution (PSD) and temperature (T), are developed using in-situ microphysical measurements at low and mid-latitudes, remote sensing data, and model results. The ratio $[\frac{IWC}{\sigma}]$, proportional to r_e, increases with T. Lower values of $[\frac{IWC}{\sigma}]$ are observed near cloud top and base than within a cloud layer, although $[\frac{IWC}{\sigma}]$ changes more with temperature than relative height within the cloud. For equivalent radar reflectivities (Z_e) below about -28 dB, the minimum detectable with forthcoming spaceborne cloud radar, $[\frac{IWC}{\sigma}]$ is a nearly constant value. IWC increases almost linearly with σ, with a temperature-dependence noted. **Citation:** Heymsfield, A. J., D. Winker, and G.-J. van Zadelhoff (2005), Extinction-ice water content-effective radius algorithms for CALIPSO, *Geophys. Res. Lett.*, *32*, L10807, doi:10.1029/2005GL022742.

1. Introduction

[2] Forthcoming spaceborne lidar and cloud (94 GHz) radar offer an opportunity to quantitatively evaluate representations of clouds in global climate models (GCM) and to provide global surveys of vertical profiles of cloud microphysical properties [*Stephens et al.*, 2002]. An advantage of spaceborne lidar over radar is its ability to detect optically thin clouds. A spaceborne lidar beam, however, is completely attenuated after penetrating a cumulative optical depth of about 3 and cannot provide information through moderate to thick cloud layers that radar can.

[3] If spaceborne lidar and radar are to reach their potential usefulness, their measurements must be converted to one or more GCM-modeled prognostic variables. The lidar-radar approach [*Intrieri et al.*, 1993], combining coincident measurements synergistically, provides retrieval of IWC, a GCM-prognostic variable, better than could be derived from either measurement alone. This has led to launching CALIPSO lidar and CloudSat radar together so that they collect nearly coincident data. Because lidar can detect radiatively significant thin cirrus missed by radar [*McGill et al.*, 2004] algorithms deriving IWC and other GCM variables from lidar measurement are required.

0094-8276/05/2005GL022742$05.00

[4] PSD and particle shape determinations can yield both IWC and σ: IWC is roughly related to the cube of the diameter and σ to its square. The ratio $[\frac{IWC}{\sigma}]$ is therefore a function of the form of the PSD; often a function of temperature and, to a much lesser extent, of number concentration. The effective radius, r_e is used to prescribe cloud radiative properties and is given by $c[\frac{IWC}{\sigma}]$, where c is 1.64 for ice particles of any shape according to *Foot* [1988].

[5] Figure 1 shows the wide range of $[\frac{IWC}{\sigma}]$ observed with T. Its lowest values are from the first to derive it from direct measurements of IWC and σ [*Garrett et al.*, 2003]. No method exists to directly measure $[\frac{IWC}{\sigma}]$ or r_e from a single probe. Most other values in the figure have been indirectly derived using measurements of PSD and estimates of particle mass or cross-sectional area (A_c). It has also been derived indirectly from radar/lidar remote sensing [*van Zadelhoff et al.*, 2004].

[6] The study reported herein uses in-situ data, remote sensing, and microphysical modeling to examine the relationship between σ as derived from lidar backscatter measurements, to the IWC. Section 2 discusses the data set and instruments, and Section 3 characterizes how $[\frac{IWC}{\sigma}]$ varies with T, height in the cloud layer, and radar reflectivity. Section 4 summarizes the primary findings.

2. Methods

[7] This study uses data acquired from several field programs, with the following conditions, sources, and derivations of the data.

[8] 1) Low latitude deep convection, Cirrus Regional Study of Tropical Anvils and Cirrus Layers (CRYSTAL) Florida Area Cirrus Experiment (FACE). More than 11000, 5 sec data points from twelve flights from the University of North Dakota Citation, the majority from between -55 and 0°C, and more than 4000 from six flights by the NASA WB57 aircraft, from -75 to -55°C. Direct measurements of σ and IWC [*Garrett et al.*, 2003] and those parameters derived from PSD and particle shapes (A. J. Heymsfield et al., Effective radius of ice cloud particle populations derived from aircraft probes, submitted to *Journal of Atmospheric and Oceanic Technology*, 2005) (hereinafter referred to as H05) are obtained.

[9] 2) Thin, tropical ice clouds near Fiji, Central Equatorial Pacific Experiment (CEPEX). Smaller number of data points, indirectly acquired between -40 and -30°C, including data in small particle sizes [*Heymsfield and McFarquhar*, 1996]

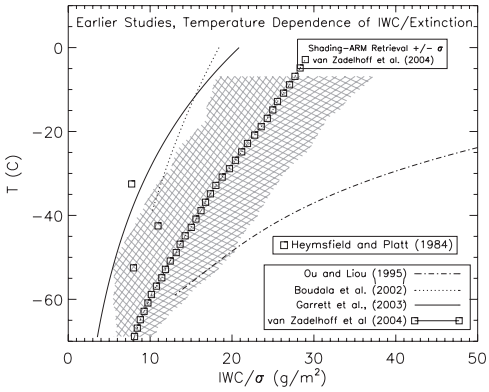

Figure 1. Estimates of the ratio $[\frac{IWC}{\sigma}]$ from earlier studies as a function of temperature.

[10] 3) Mid-Latitude, synoptically generated cirrus (FIRE-2), near Coffeyville, Kansas. Vertical profiles of σ and IWC obtained indirectly from balloon-borne replicators between −65 and −35°C [*Miloshevich and Heymsfield*, 1997].

[11] 4) σ and IWC are derived primarily from PSDs by indirect method (H05). PSD in small, (<50 μm) sizes estimated from forward scattering spectrometer (FSSP)-type electronic probes (CRYSTAL-FACE) and impaction probes (CEPEX and FIRE-2). FSSP particles are assumed to be solid ice spheres. For larger particles the sizes and areas are from 2-D type imaging probes. Accurate IWCs are determined from the PSD using particle densities derived from the direct IWC measurements (H05). Based on the analysis given by H05, the PSD probes are considerably more sensitive than the direct probes to IWC and σ, have σ values about 1/2 of measured at the same time, and have been suggested to provide more accurate σ than measured.

[12] 5) Model: the particle growth model considers cloud condensation nuclei (CCN) from initialization at a relative humidity (RH) of 60% with respect to water, to haze particle formation and activation of cloud droplets followed by homogeneous nucleation and subsequent growth (H05). Fixed vertical velocities are used to examine $[\frac{IWC}{\sigma}]$ over a range of temperatures. The model distribution of CCN is relatively unimportant (H05). Ice particle fallout is not considered, therefore, model results are relevant to early cirrus formation or their upper parts.

3. Results

[13] As Figure 2 shows, between −70 and 0°C the ratio, $[\frac{IWC}{\sigma}]$, increases by about a factor of four for each data set and ten for all data sets together, and, with values comparable to earlier indirect estimates; r_e are about 64% larger than $[\frac{IWC}{\sigma}]$. The data from all projects and from the remote sensing approach are consistent at the lower temperatures. Although point values of σ are higher for the direct measurements (not shown), the probe's higher detection threshold yields the result that only relatively small values of $[\frac{IWC}{\sigma}]$ are captured. This would influence data for the lower temperatures sampled predominantly by the WB57. For warmer temperatures, Citation values for $[\frac{IWC}{\sigma}]$ from indirect measurements are larger than other data sets. We attribute this to the Citations sampling conditions: thick, convectively-produced ice cloud layers, relatively warm temperatures, and large, high mass particles. These conditions shift the distribution of ice mass to area upwards. This may not be captured by remote sensing data, requiring coincident (ground-based) lidar and radar, because lidar is not likely to penetrate the deep, thick anvil cloud sampled by the Citation. Consequently, values of $[\frac{IWC}{\sigma}]$ in anvil cirrus may in fact be lower than those obtained from remote sensing. The $[\frac{IWC}{\sigma}]$ values from the direct (cloud integrating nephelometer (CIN)) measurements at the warmer temperatures sampled by the Citation fall near the left edge of the shaded, remotely sensed data, about 1/2 of the indirect values. The discrepancy noted between the Citation and other measurements are not of concern here because a lidar beam is unlikely to penetrate layers of large σ.

[14] The model used produces ice particles solely through homogeneous nucleation, an upper-bound on ice concentrations produced in synoptically generated cirrus. Once nucleated, they grow and deplete the water vapor, simulating initial cirrus formation. Figure 2 shows the model results at the endpoints of parcel runs initiated between −32 and −70°C, and lifted slowly at 5 and 20 cm/s, at that point where all water vapor density excess has been depleted. The IWC is almost completely given by the initial temperature and water vapor excess; and σ by the number of particles nucleated, a function of the temperature and vertical velocity. The model $[\frac{IWC}{\sigma}]$ increases with temperature in a way that roughly conforms to observations over the same temperature range. Higher vertical velocity generates smaller, more numerous particles with larger IWC and smaller $[\frac{IWC}{\sigma}]$. The discrepancy between the model σ and those observed are the result of model ice concentrations from 1 to 10 cm^{-3}, about ten times larger than for aged cirrus. For anvil cirrus, transport of condensate from below in vigorous convective updrafts will influence the temperature dependence of $[\frac{IWC}{\sigma}]$.

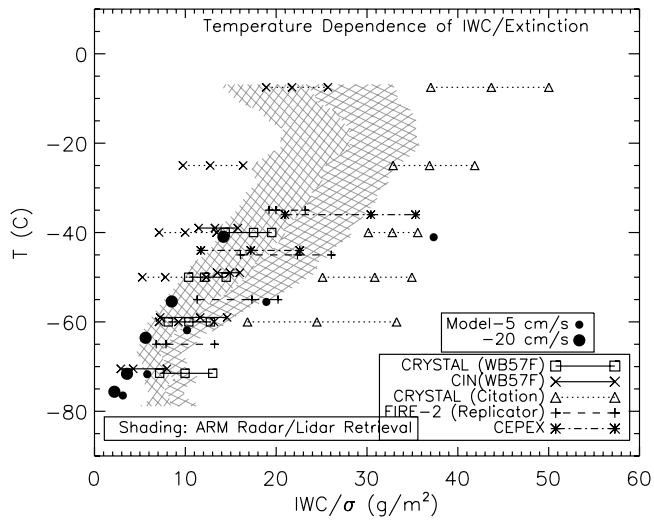

Figure 2. Temperature dependence of $[\frac{IWC}{\sigma}]$ from CRYSTAL-FACE, FIRE-2, and CEPEX. Horizontal bars are plotted at the mid-point of a temperature interval. Along each horizontal bar corresponding to a temperature interval, the left, center and right points along each bar are the 25th, 50th, and 75th percentiles of $[\frac{IWC}{\sigma}]$.

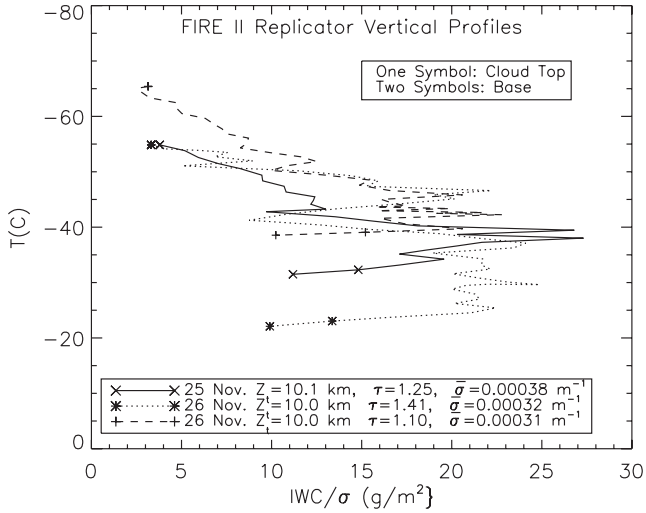

Figure 3. FIRE-2 replicator observations of $[\frac{IWC}{\sigma}]$ as a function of temperature. Cloud layer mean σ and integrated σ to yield optical depth are listed.

[15] Synoptically-generated ice cloud layers are characterized by relatively smaller particles near cloud top, larger particles in mid-and lower levels through particle growth and size sorting, and smaller particles near the bottom of the cloud resulting from sublimation [*Miloshevich and Heymsfield*, 1997]. This vertical size structure leads to increasing $[\frac{IWC}{\sigma}]$ from cloud top to near cloud base, followed by a decrease to the base itself. The question of whether $[\frac{IWC}{\sigma}]$ is related to its height in the cloud layer was investigated using three vertical profiles from balloon-borne replicator ascents in cirrus with optical depths of about 1 and Lagrangian spiral descents by the CRYSTAL-FACE aircraft. The tendency for $[\frac{IWC}{\sigma}]$ to increase from cloud top to close to its base was noted (Figure 3). Cloud top and base values were about 1/2 of those from mid-and lower cloud. For the four Citation spirals in very deep layers, spanning a temperature range of 20°C, the downward increase was closer to 25%. There was also little change in $[\frac{IWC}{\sigma}]$ in a cold case sampled by the WB57 off the coast of Nicaragua. It would seem from these spirals, many from earlier field programs, and from remote sensing observations [*van Zadelhoff et al.*, 2004], changes in $[\frac{IWC}{\sigma}]$ are related to temperature, but that the vertical height within the cloud layer is also important.

[16] In order to specify $[\frac{IWC}{\sigma}]$ in cloud situations detectable by lidar but not by radar, a relationship between Z_e at 94 GHz and $[\frac{IWC}{\sigma}]$ is required. Z_e calculated here uses Mie scattering calculations for a radar frequency of 94 GHz [*Heymsfield et al.*, 2005] and is probably accurate to about 3 dB. There is a general increase in $[\frac{IWC}{\sigma}]$ with Z_e (Figure 4). Some of the variability shown by the width of the error bars in the figure is due to temperature variation. In general, however, increasing Z_e is correlated with increasing temperature. Taking −28 dBZ$_e$ as the detection threshold for the CloudSat radar, $[\frac{IWC}{\sigma}]$ has a mean of about 10 g/m^2 for cloud layers below its detection threshold. From the direct measurements, $[\frac{IWC}{\sigma}]$ for Z_e below −28 dB are about 40% as large.

[17] To further investigate the temperature dependence of the σ−IWC relationship, the two variables have been plotted against each other and partitioned by temperature for each of the data sets investigated (Figure 5a). With temperature (color shift from blue to red), IWC increases more rapidly than σ, leading to the increase in $[\frac{IWC}{\sigma}]$ with temperature. (Constant $[\frac{IWC}{\sigma}]$ is given by the sloping lines in the figure). Remote sensing retrievals yield a similar trend. At low σ, however, the median leads to higher $[\frac{IWC}{\sigma}]$. This is an artifact produced by the necessity to sample radar-detectable, relatively high IWC regions. The model calculations show a similar temperature trend for reasons stated earlier, but with higher values for a given IWC. Figure 5b gives individual σ and IWC values in one of the color ranges from Figure 5a. The progressive shift with temperature reflects the increasing IWC and thus the higher $[\frac{IWC}{\sigma}]$. To a lesser extent, the increase in σ mimics the model results. The figure also gives median values for σ in intervals of IWC showing that $[\frac{IWC}{\sigma}]$ increases with increasing temperature and IWC. The median values quite closely agree with the median values derived from the remote sensing method. In these calculations, the curve from *Heymsfield and McFarquhar* [1996], using a broad set of CEPEX data, falls above our median curve where σ are small because only data from the large particle probe was used. At large σ, the correspondence is excellent. A power-law, least-squares curve that relates σ (m^{-1}) and IWC (g/m^3) has been generated using the median values for σ from the in-situ data as a function of IWC intervals shown in Figure 5b:

$$IWC = a\sigma^b,$$

where a = 119 and b = 1.22, with correlation coefficient = 0.997. Had the direct measurements of σ been used, this curve would shift downward such that a given σ would predict an IWC which is about 1/3 of the value (for σ above the probe's detection threshold) derived from the indirect measurements with a tendency for improved agreement as σ decreases. *Platt* [1997] shows power-law fits to earlier observations.

[18] For a given a value of σ, there is a progressive increase in IWC with temperature observed in the aircraft and radar-lidar remote sensing data sets noted above.

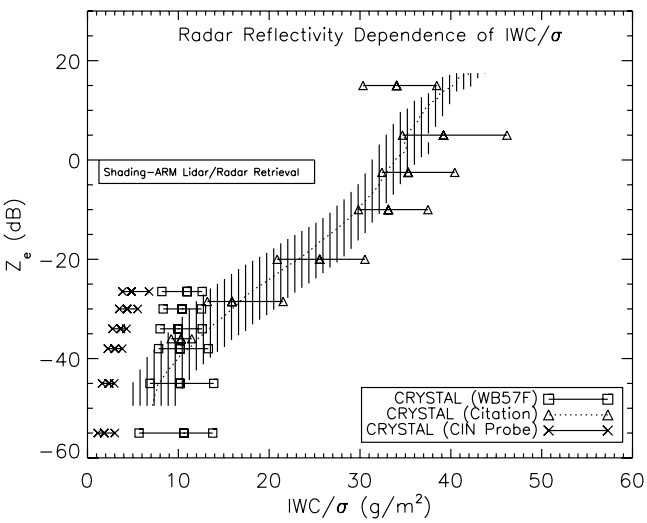

Figure 4. Same as Figure 2, radar reflectivity instead of temperature.

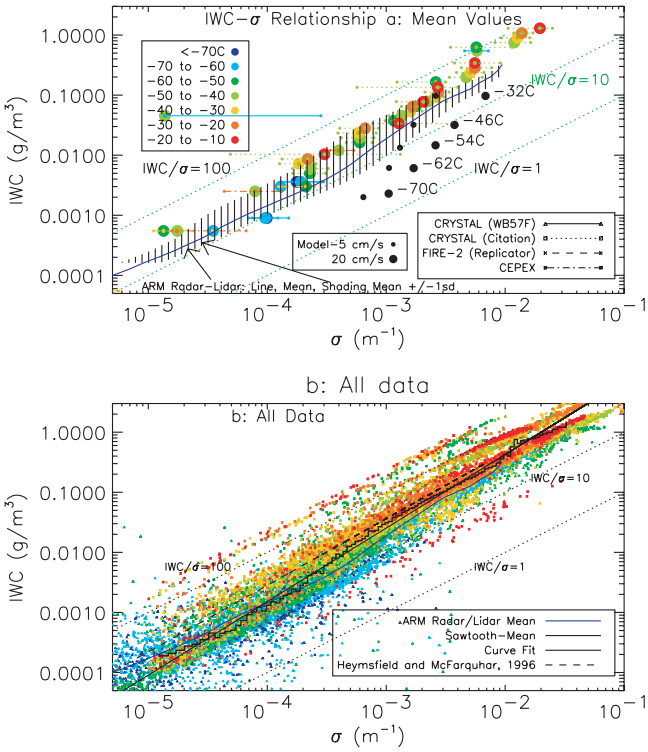

Figure 5. Relationship between σ and IWC derived from various data sets. (a) Mean values. (b) Individual data points, mean in given intervals, and power-law curve fitted through the mean values.

Temperature dependence is captured by dividing the aircraft data set in 10°C increments between −80 and −10°C through the following relationships:

$$a = 89 + 0.6204(^{\circ}C), b = 1.02 - 0{:}00281T(^{\circ}C).$$

4. Summary and Conclusions

[19] This study reports the development of algorithms for retrieving IWC and effective radius from spaceborne and ground-based lidar measurements. It focuses on those cloud regions where the radar reflectivity falls below its threshold detection level and the combined lidar/radar retrieval scheme cannot be used. It is found that the ratio $[\frac{IWC}{\sigma}]$ increases from about 5 to 40 g/m^2 as temperatures increase from −70 and 0°C. The r_e is about 64% larger than $[\frac{IWC}{\sigma}]$. The effects of relative height within the cloud layer is also important. Because remote sensing results suggest different temperature parameterizations for different locations, the generality of these results must be established using data from a wide range of geographic locations.

[20] Perhaps the most important result of this study is that, for cloud layers below the CloudSat 94 GHz radar detection threshold of about −28 dBZ$_e$, $[\frac{IWC}{\sigma}]$ is about 10 g/m^2. This result must be confirmed from measurements in those thin cirrus layers that may be important to the Earth's radiation budget. Such cloud layers are amenable to sampling by spaceborne lidar.

[21] A relationship between σ and IWC is developed, which includes temperature information. On average, lower temperatures have lower IWC values and higher temperatures higher ones.

[22] Our study uses an indirect method for deriving σ and IWC from size distributions and A_c derived from particle probes. Had the direct measurements been used [see *Garrett et al.*, 2003], σ would have been about twice as large as given by the indirect method. The direct measurements would give about 1/2 to 1/3 of the IWC for the same σ, with closer values found as σ decreased to the probe's detection threshold. If the measurements are accurate, future studies should use direct measurements of σ. Because small particles dominate extinction in situations amenable to lidar estimates of the IWC, the measurements of small particles from size spectrometers also requires improvements because currently they are capable of obtaining lower values of σ.

[23] **Acknowledgments.** This research was supported by the CALIPSO Project, the Mesoscale and Microscale Division of NCAR, and the NASA CRYSTAL-FACE program through NASA-NSF agreement number W-10, 024, Hal Maring program manager. This research was also supported through the SRON Program Bureau External Research (EO-052).

References

Boudala, F. S., G. A. Isaac, Q. Fu, and S. G. Cober (2002), Parameterization of effective ice particle size for high latitude clouds, *Int. J. Climatol.*, *22*, 1267–1284.

Foot, J. S. (1988), Some observations of the optical properties of clouds. Part II: Cirrus, *Q. J. R. Meteorol. Soc.*, *114*, 145–164.

Garrett, T. J., H. Gerber, D. G. Baumgardner, C. H. Twohy, and E. M. Weinstock (2003), Small, highly reflective ice crystals in low-latitude cirrus, *Geophys. Res. Lett.*, *30*(21), 2132, doi:10.1029/2003GL018153.

Heymsfield, A. J., and C. M. R. Platt (1984), A parameterization of the particle size spectrum of ice clouds in terms of the ambient temperature and ice water content, *J. Atmos. Sci.*, *41*, 846–855.

Heymsfield, A. J., and G. M. McFarquhar (1996), On the high albedos of anvil cirrus in the tropical Pacific warm pool: Microphysical interpretations from CEPEX and from Kwajalein, Marshall Islands, *J. Atmos. Sci.*, *53*, 2424–2451.

Heymsfield, A. J., Z. Wang, and S. Matrosov (2005), Improved radar ice water content retrieval algorithms using coincident microphysical and radar measurements, *J. Appl. Meteorol.*, in press.

Intrieri, J. M., G. L. Stephens, W. L. Eberhard, and T. Uttal (1993), A Method for determining cirrus cloud particle sizes using lLidar and radar backscatter technique, *J. Appl. Meteorol.*, *32*, 1074–1082.

McGill, M. J., L. Li, W. D. Hart, G. M. Heymsfield, D. L. Hlavka, P. E. Racette, L. Tian, M. A. Vaughan, and D. M. Winker (2004), Combined lidar-radar remote sensing: Initial results from CRYSTAL-FACE, *J. Geophys. Res.*, *109*, D07203, doi:10.1029/2003JD004030.

Miloshevich, L. M., and A. J. Heymsfield (1997), A balloon-borne continuous cloud particle replicator for measuring vertical profiles of cloud microphysical properties: Instrument design, performance, and collection efficiency analysis, *J. Atmos. Oceanic Technol.*, *14*, 753–768.

Ou, S., and K.-N. Liou (1995), Ice microphysics and climate temperature feedback, *Atmos. Res.*, *35*, 127–138.

Platt, C. M. R. (1997), A parameterization of the visible extinction coefficient of ice clouds in terms of the ice/water content, *J. Appl. Meteorol.*, *54*, 2083–2097.

Stephens, G. L., et al. (2002), The CloudSat mission and the EOS constellation: A new dimension of space-based observations of clouds and precipitation, *Bull. Am. Meteorol. Soc.*, *83*, 1771–1790.

van Zadelhoff, G.-J., D. P. Donovan, H. Klein Baltink, and R. Boers (2004), Comparing ice cloud microphysical properties using CloudNET and Atmospheric Radiation Measurement Program data, *J. Geophys. Res.*, *109*, D24214, doi:10.1029/2004JD004967.

A. J. Heymsfield, National Center for Atmospheric Research, 3450 Mitchell Lane, Boulder, CO 80301, USA. (heyms1@ucar.edu)

G.-J. van Zadelhoff, Koninklijk Nederlands Meteorologisch Instituut, P.O. Box 201, NL-3730 AE De Bilt, Netherlands. (zadelhof@knmi.nl)

D. Winker, MS/435, Atmospheric Sciences Division, NASA Langley Research Center, Hampton, VA 23681, USA. (david.m.winker@nasa.gov)